NJC

ROYAL SOCIETY OF CHEMISTRY

PAPER

View Article Online
View Journal | View Issue

Check for updates

Cite this: *New J. Chem.*, 2020, 44, 13259

Chromogenic and fluorogenic "off–on–off" chemosensor for selective and sensitive detection of aluminum (Al^{3+}) and bifluoride (HF_2^-) ions in solution and in living Hep G2 cells: synthesis, experimental and theoretical studies†

Samit Pramanik,[a] Saikat Kumar Manna,[b] Sudipta Pathak, *[b] Debasish Mondal,[c] Kunal Pal[d] and Subrata Mukhopadhyay[a]

Received 27th April 2020,
Accepted 7th July 2020

DOI: 10.1039/d0nj02117b

rsc.li/njc

A simple pyridine-dicarbohydrazide based colorimetric and fluorometric chemosensor **L** was designed and synthesized for Al^{3+} ion sensing in organo aqueous solution. In the presence of Al^{3+} ions, probe **L** exhibited visible color changes and fluorescence enhancement (20-fold) due to Al^{3+} induced chelation-enhanced fluorescence (CHEF) effects. Chemosensor **L** revealed high selectivity toward Al^{3+} ions by "turn-on" fluorescence among the other competitive metal ions examined with a detection limit of 0.8 μM. Probe **L** was found to bind with Al^{3+} ions in a 1 : 2 (probe : metal) stoichiometric fashion, with an association constant (K_a) of 4.26×10^4 M^{-2}. In addition, DFT and TDDFT calculations were carried out to recognize the binding nature and electronic properties of probe **L** and its Al-complex. Furthermore, the *in situ* prepared [**L**–Al] complex was able to detect HF_2^- anions *via* a metal displacement strategy. The bioimaging application of Al^{3+} and HF_2^- was implemented in living human liver cancer cells (Hep G2).

Published on 10 July 2020. Downloaded by N-List College Programme on 9/9/2020 6:54:20 AM.

Introduction

Being the third most abundant (8.3% by weight) element (after oxygen and silicon) on the surface of the earth, aluminum is widely associated with our daily contemporary life in the form of food packaging, water purification, cooking utensils, pharmaceuticals, manufacturing of computers, *etc.*[1–3] Aluminium compounds are also extensively used in the paper industry, in dye production, in the textile industry, and as a component of many cosmetic preparations, and are currently utilized in the alimentary industry and in many more.[4,5] Therefore, there is a good chance of accumulation of aluminum ions (Al^{3+}) in the food chain and toxicity towards human health. But, the tolerable daily intake of aluminum is about 3–10 mg and consequently the upper limit of aluminum nutritional intake is about 7 mg per kg of body weight per week according to a WHO report.[6] Excess accumulation of this metal causes some serious diseases like myopathy, Parkinson's disease, Alzheimer's disease, osteoporosis, headaches, anemia, chronic renal failure, dialysis encephalopathy, bone softening, kidney damage and even breast cancer.[7–9] The solubility of aluminium minerals at lower pH increases the amount of available Al^{3+}, which can affect plants' normal growth and development, ultimately hampering agricultural production.[10] Therefore, easy detection of aluminum ions is imperative in various samples connected to the environment, foodstuffs, medicine, *etc.* But detection of aluminium ions is still a major challenge due to their low coordination capability, high hydration aptitude and lack of spectroscopic features.[11] A number of analytical techniques have been used for the detection of aluminum ions, such as atomic absorption spectrometry,[12] inductively coupled plasma atomic emission spectrometry (ICP-AES),[13,14] inductively coupled plasma mass spectrometry (ICP-MS),[15] nanoparticle-based sensors,[16] ion selective membranes,[17] electrochemical methods,[18] and several other methods.[19] But these techniques are restricted to the laboratory because of high equipment cost, time consuming nature and the necessity for trained personnel. However, spectrofluorimetry is superior in terms of quick analysis, high selectivity, sensitivity and ease of operation. As Al^{3+} is a hard acid, it prefers hard base donor sites for coordination,[20] so Schiff base probes with N and O donor centres could be used as good ligands for

[a] *Department of Chemistry, Jadavpur University, Kolkata 700032, India*
[b] *Department of Chemistry, Haldia Government College, Debhog, Purba Medinipur, West Bengal, India. E-mail: sudiptachemster@gmail.com; Tel: +91-8001317336*
[c] *School of Chemistry and Biochemistry, Thapar Institute of Engineering and Technology, Patiala 147004, Punjab, India*
[d] *Department of Life Science and Biotechnology, Jadavpur University, Kolkata 700032, India*

† Electronic supplementary information (ESI) available. CCDC 1979155. For ESI and crystallographic data in CIF or other electronic format see DOI: 10.1039/d0nj02117b

Published on 10 July 2020. Downloaded by N-List College Programme on 9/9/2020 6:54:20 AM.

Al^{3+} detection.[21] In several research fields hydrazides have been extensively used as ligands due to their facile syntheses, tunable electronic properties and good chelating capability.[22] In this work, we have designed and synthesized a pyridine-dicarbohydrazide based 'turn-on' chemosensor **L** which shows high selectivity for Al^{3+} with a low detection limit (LOD).

Anions play a vital role in the area of supramolecular chemistry, especially in environmental, chemical, medical and biological systems. Among the different anions, recognition of semi-ionic, three-center, and four-electron bonding bifluoride ions (HF_2^-) is of growing interest because of their extensive applications in various fields including etching of borosilicate glass capillary columns, insecticides, fluorometric detection of ultra-trace levels of beryllium in occupational hygiene samples, and preparation of borane derivatives and molten salts.[23] Until now, very few chemosensors have been reported for bifluoride ions.[24] Therefore, there is an urgent requirement for fluorescent and biocompatible probes that can selectively and sensitively detect bifluoride ions with a rapid response through easy spectral analysis. However, the design and development of fluorescent chemosensors for anions in aqueous solution is still a difficult task due to the strong hydration properties of anions. This problem could be evaded by using the metal displacement strategy. Keeping this in mind, we report here a displacement-based sensing system by using an Al^{3+}-based ensemble (**L**–$2Al^{3+}$) for bifluoride ion recognition. It is noteworthy to mention that chemosensor **L** has interesting analytical features like its easy synthetic route with good yield and reasonably low detection limit for Al^{3+} ions with no interference from a number of cations in comparison to reported methods (Table S1, ESI†). Another notable aspect of the **L**–$2Al^{3+}$ complex is that it displays a good reversible fluorescence response to HF_2^-. Furthermore, probe **L** is effectively applied to image Al^{3+} and HF_2^- ions in cultured Hep G2 cells.

Results and discussion

Scheme 1 outlines the synthetic route of chemosensor **L**. Compound **1** was prepared following a literature procedure.[25] Probe **L** was then synthesized by the condensation reaction between compound **1** and

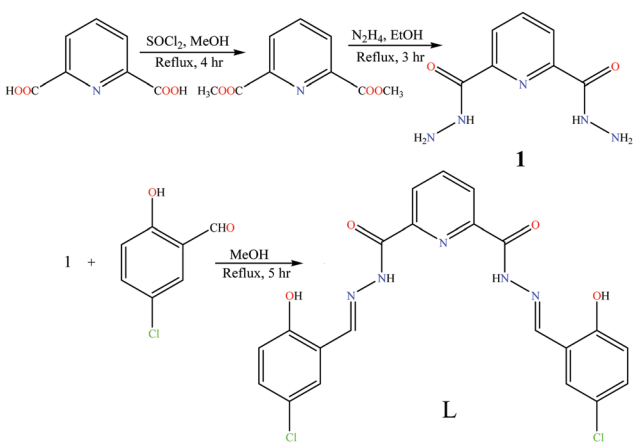

Scheme 1 Chemical structure and synthetic route of **L**.

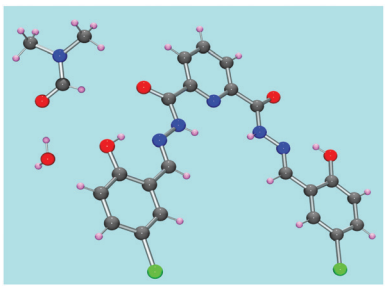

Fig. 1 ORTEP view of molecular probe **L** (with 40% probability).

2-hydroxy-4-chlorobenzaldehyde with 84% yield. The molecular structure of **L** was confirmed by ^1H NMR, ^{13}C NMR, ESI-MS, FT-IR and also by single-crystal X-ray diffraction analysis (Fig. 1 and Table S2, ESI†).

The spectroscopic properties of probe **L** were investigated by monitoring absorption and fluorescence changes in the presence of several metal ions, such as K^+, Na^+, Mg^{2+}, Ca^{2+}, Pb^{2+}, Pd^{2+}, Cd^{2+}, Hg^{2+}, Zn^{2+}, Cu^{2+}, Al^{3+}, Ag^+, Fe^{2+}, Co^{2+}, Ni^{2+} and Mn^{2+} in DMSO : H_2O (8 : 2, v/v, 10 mM HEPES buffer, pH 7.4) solution at room temperature. As illustrated in Fig. 2, free probe **L** displayed a maximal absorption peak at 345 nm, which corresponds to a π–π^* transition from the conjugated moiety of **L**. However, upon gradual addition of Al^{3+} ions to the solution of **L**, the initial absorption band at 345 nm decreased and a simultaneous increase at 402 nm with a red shift of 57 nm was observed, accompanied by a naked eye color change from colorless to light yellow. The clear isosbestic point at 370 nm undoubtedly indicates the formation of an Al^{3+} complex in the binary mixture. Again, chemosensor **L** did not exhibit any noteworthy changes in absorption spectra with the addition of a number of competitive metal ions, signifying the high selectivity of this probe for Al^{3+} ions. To investigate the suitable pH range in which sensor **L** can effectively detect Al^{3+}, a pH titration of **L** was carried out (Fig. S15, ESI†). It is noteworthy to mention that addition of Al^{3+} resulted in a high absorbance in a pH range of 6 to 9. When the pH is greater than 9, the absorbance is decreased due to the formation of colloidal $Al(OH)_3$. These observations indicate that the pH range of 6 to 9 is suitable for monitoring Al^{3+} by chemosensor **L**.

As shown in Fig. 3, in the absence of Al^{3+} ions, probe **L** showed a very weak emission band centred at 483 nm (λ_{ext} = 371 nm) in

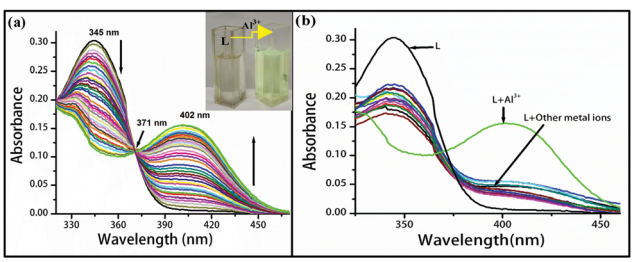

Fig. 2 (a) The UV-vis absorption spectra of **L** ($c = 2 \times 10^{-4}$ M) in the presence of Al^{3+} ($c = 2 \times 10^{-5}$ M) ions in DMSO–H_2O (8 : 2, v/v, 10 mM HEPES buffer, pH 7.4) solution. Inset: Color change after addition of Al^{3+} to probe **L**. (b) Absorption spectra of **L** in the presence of different metal ions.

 This journal is © The Royal Society of Chemistry and the Centre National de la Recherche Scientifique 2020

Published on 10 July 2020. Downloaded by N-List College Programme on 9/9/2020 6:54:20 AM.

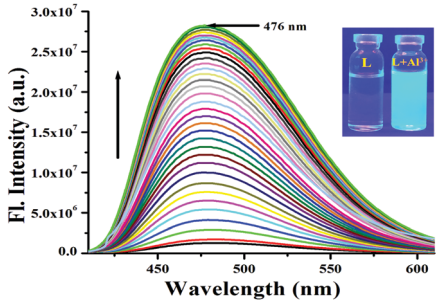

Fig. 3 Changes in the fluorescence spectra of **L** ($c = 2 \times 10^{-4}$ M) in the presence of different amounts of Al^{3+} ($c = 2 \times 10^{-5}$ M) ions in DMSO–H_2O (8 : 2, v/v, 10 mM HEPES buffer, pH 7.4) solution. Inset: Fluorescence change after addition of Al^{3+} to probe **L**.

DMSO–H_2O (8 : 2, v/v, 10 mM HEPES buffer, pH 7.4). This weak emission of probe **L** is due to the (a) excited state intramolecular proton transfer (ESIPT) from the –OH group to the imine nitrogen; (b) photoinduced electron transfer effect from the lone pair of the imine nitrogen and (c) isomerization of the –HC═N (imine) bond.[26] However, treatment of probe **L** with 3 equivalents of Al^{3+} ions induced a gradual increase in fluorescence (20-fold) along with a blue shift of 7 nm, having the highest emission intensity at 476 nm and a color change from dark to greenish-blue under UV light. This significant fluorescence 'turn-on' in the presence of Al^{3+} ions might be explicated by the formation of a complex between probe **L** and Al^{3+} through the coordination of two "O" and one "N" atom. This inhibits both the ESIPT and PET processes as well as C═N isomerization, resulting in a distinctive chelation enhanced fluorescence (CHEF) effect. In order to explore the practical applicability, the pH effects on the fluorescence response of probe **L** in the absence and presence of Al^{3+} were examined. Fig. S16 (ESI†) shows that **L** is weakly emissive in a wide range of pH (3–13). The low emission intensity of the **L**–Al^{3+} complex at pH < 6 was presumably due to the free **L** that remains uncoordinated to Al^{3+}. At pH > 9, Al^{3+} is converted to $Al(OH)_3$ and $Al(OH)_4^-$, leaving the sensor almost in its free anionic form in the solution. At pH ~ 7 the sensor is deprotonated and the resulting dianionic ligand forms a chelate with Al^{3+}, leading to fluorescence enhancement *via* the CHEF mechanism (Scheme 2). Therefore, sensor **L** is capable of being used for selective detection of Al^{3+} at physiological pH, and can be a suitable candidate for biological applications.

Additionally, ^{1}H NMR titration was performed by gradual addition of a nitrate salt of Al^{3+} ions to a DMSO-d_6 solution of **L** (Fig. 4).

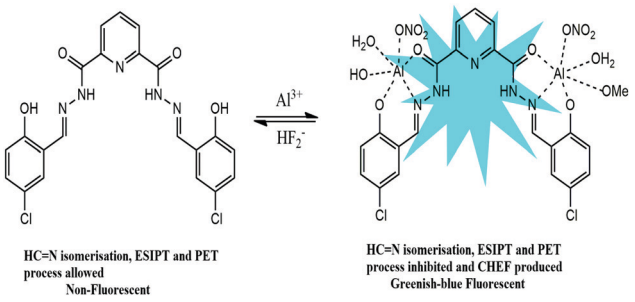

Scheme 2 Proposed sensing mechanism for detection of Al^{3+} by probe **L**.

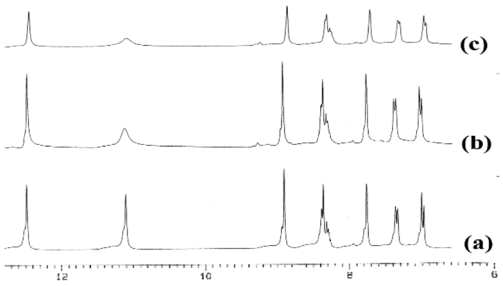

Fig. 4 ^{1}H NMR spectra in DMSO-d_6: (a) **L** only, (b) **L** and 1 equiv. of Al^{3+} and (c) **L** and 2 equiv. of Al^{3+}.

The result shows that the intensity of the proton signal corresponding to the hydroxyl group (–OH) at 11.08 ppm, which is the most probable binding site for Al^{3+} ions, decreases significantly relative to that of other protons upon exposure to Al^{3+} ions.

For chemosensor **L**, the IR spectrum (Fig. S4, ESI†) shows ν(OH), 3472(s); ν(NH), 3248(s); ν(C═O), 1657(s); ν(C═N), 1621 cm^{-1}. On the other hand, the IR spectrum of the **L**–Al^{3+} complex (Fig. S6, ESI†) shows a shifted frequency value and a new signal for NO_3^- at 1349 cm^{-1}. The spectrum shows ν(NH), 3189(s); ν(C═O), 1672(s); ν(C═N), 1617 cm^{-1}, but ν(OH) appears as a broad signal at 3449 cm^{-1}. This result shows that the –OH is the most probable binding site for Al^{3+} ions.

The Job plot revealed that 1 : 2 stoichiometry is the most probable binding mode between **L** and Al^{3+} ions (Fig. S10, ESI†). To attain such a type of stoichiometry, imine nitrogen, carbonyl oxygen and phenolic oxygen atoms are the most likely binding sites for Al^{3+} ions (Scheme 2). The association constant (K_a) of **L** for Al^{3+} was calculated from the Benesi–Hildebrand equation[27] on the basis of fluorometric titration as 4.26×10^4 M^{-2} (Fig. S12, ESI†). The selectivity of chemosensor **L** towards different metal cations was examined under identical working conditions. As shown in Fig. 5, probe **L** demonstrated a strong fluorescence response at 476 nm, while the other cations [K^+, Na^+, Mg^{2+}, Ca^{2+}, Pb^{2+}, Pd^{2+}, Cd^{2+}, Hg^{2+}, Zn^{2+}, Cu^{2+}, Ag^+, Fe^{2+}, Co^{2+}, Ni^{2+} and Mn^{2+}] did not cause any remarkable emission spectral changes. In order to further evaluate the practical capability of probe **L** as an Al^{3+} selective fluorescent chemosensor, we conducted competitive experiments on addition of Al^{3+} ions to a solution of **L** in the presence of excess equivalents of other individual competitive metal ions. The increase in fluorescence intensity induced by

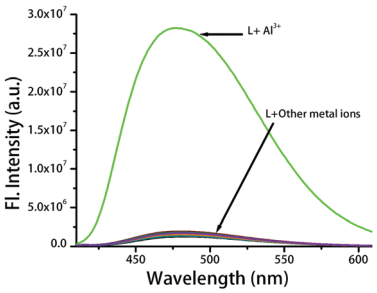

Fig. 5 Fluorescence response of **L** ($c = 2 \times 10^{-4}$ M) to different metal ions in DMSO–H_2O (8 : 2, v/v, 10 mM HEPES buffer, pH 7.4) solution (λ_{ext} = 370 nm).

Published on 10 July 2020. Downloaded by N-List College Programme on 9/9/2020 6:54:20 AM.

mixing Al^{3+} ions with other miscellaneous cations was comparable to that elicited by Al^{3+} alone, indicating stable complexation between **L** and Al^{3+}. The above results indicate high selectivity of probe **L** for Al^{3+} over other commonly coexistent cations in organo-aqueous solution. The fluorescence intensity of **L** at 476 nm exhibited a good linear relationship with the Al^{3+} concentration ranging from 0.99 μM to 20.6 μM, based on which the detection limit[28] for Al^{3+} was calculated to be 0.8 μM (Fig. S11, ESI†).

Reversibility is an essential feature of a probe to be used as a chemosensor to detect particular metal cations. Here, the *in situ* generated **L**–$2Al^{3+}$ complex displayed fluorescence "turn-off" behavior only in the presence of HF_2^- ions. Now, to inspect this, when an excess amount of $NaHF_2$ solution was added to the solution containing the **L**–$2Al^{3+}$ complex system, the emission band at 476 nm gradually decreased, accompanied by emission color changes from deep blue to dark (Fig. 6a). However, various common anions such as Cl^-, Br^-, AcO^-, CO_3^{2-}, N_3^-, HCO_3^-, NO_2^-, SO_4^{2-}, and $H_2PO_4^-$ did not produce any noticeable results under similar conditions except F^-. F^- ions decrease the fluorescence intensity but only by a small extent compared to HF_2^- ions (Fig. 6b). The added fluoride source (TBAF) could be hydrolyzed, and a small amount of HF_2^- may be generated *in situ* to assist the quenching of emission of the **L**–$2Al^{3+}$ complex; thus, a quenching response might be observed.[29] Such fluorometric changes were mainly due to the removal of Al^{3+} from the **L**–$2Al^{3+}$ system followed by the regeneration of probe **L** as shown in Scheme 2. These properties indicate that the **L**–$2Al^{3+}$ ensemble can be employed as an "on–off" fluorescent sensor for bifluoride ions. In addition, the reversible and reusable behavior of probe **L** was also verified by performing four alternate cycles of fluorescence titration of **L** with Al^{3+} followed by addition of HF_2^- as shown in Fig. S7 (ESI†). Moreover, from the fluorescence titration experiment, we found a good linear relationship of fluorescence intensity *versus* the HF_2^- concentration over a range of 0.99 to 6.5 μM (Fig. S8, ESI†).

However, incremental addition of HF_2^- ions into a solution of the *in situ* generated **L**–$2Al^{3+}$ complex led to a gradual decrease in the absorption band at 394 nm and a concomitant increase in the intensity of a new absorption band centered at 344 nm (Fig. S9, ESI†).

In order to know the optimized geometry of **L** and **L**–$2Al^{3+}$ and the binding interactions between probe **L** and Al^{3+}, we carried out density functional theory (DFT) calculations with the B3LYP/6-311+G(d,p) basis set using the Gaussian 16 program.[30,31] The energy optimized structures of **L** and its Al-complex are presented in Fig. 7. The highest occupied molecular orbital (HOMO) and lowest unoccupied molecular orbital (LUMO) energies and spatial distribution of **L** and **L**–$2Al^{3+}$ were also calculated (ESI†). As shown in Fig. 8, the HOMO–LUMO energy gap of probe **L** was considerably reduced from 3.83 eV (88.4 kcal mol^{-1}) to 3.16 eV (72.9 kcal mol^{-1}) in the **L**–$2Al^{3+}$ complex, establishing that **L** formed a stable complex with Al^{3+} ions and supporting the red-shift of the absorption band (λ_{max}) in the UV-vis absorption spectra.[32] Moreover, TDDFT calculations were performed on the optimized geometries to explain the electronic properties of probe **L** and its Al-complex. Table S4 (ESI†) shows the details of the vertical excitation energies, oscillator frequencies and wavelengths and from these data it was found that the computed vertical transitions were analogous to the experimentally observed UV-vis bands.

The probe was applied in Hep G2 cells (human liver cancer cell line) for fluorescence imaging of intracellular Al^{3+} ions to investigate its application in biological systems. First, Hep G2

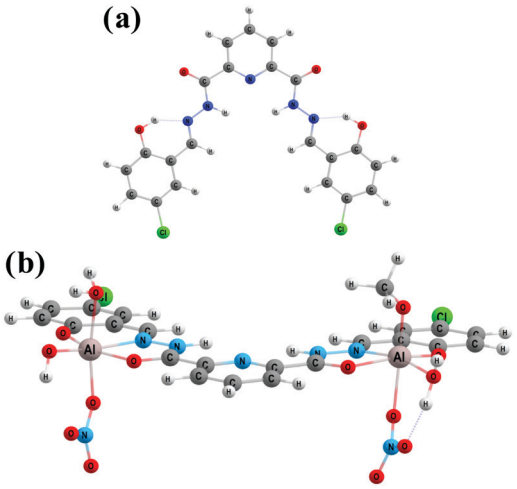

Fig. 7 The calculated energy minimized structures of **L** and the **L**–$2Al^{3+}$ complex.

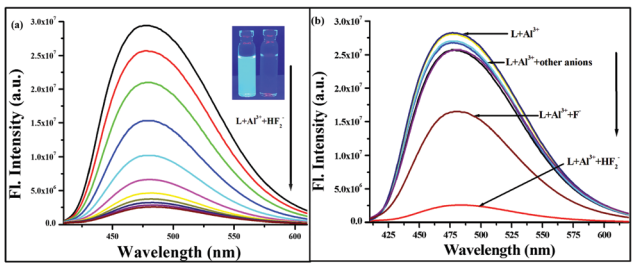

Fig. 6 (a) Fluorescence titrations of the **L**–$2Al^{3+}$ complex with a sodium salt of bifluoride in DMSO–H_2O (8 : 2, v/v, 10 mM HEPES buffer, pH 7.4) solution (λ_{ext} = 370 nm). Inset: Fluorescence photographs of **L** + Al^{3+} and **L** + Al^{3+} + HF_2^-. (b) Changes in the fluorescence spectra of the **L**–$2Al^{3+}$ complex in the presence of different anions.

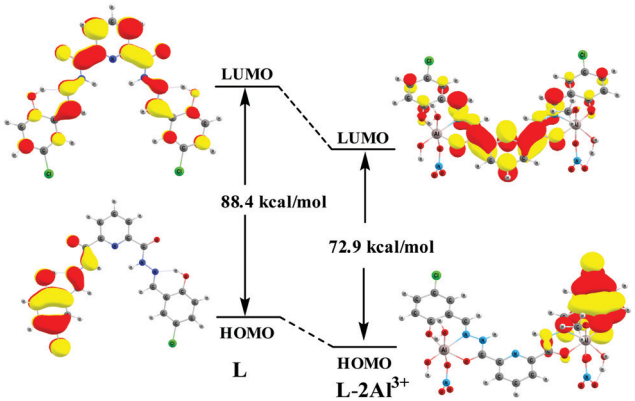

Fig. 8 HOMO and LUMO distributions of **L** and the **L**–$2Al^{3+}$ complex.

 This journal is © The Royal Society of Chemistry and the Centre National de la Recherche Scientifique 2020

Published on 10 July 2020. Downloaded by N-List College Programme on 9/9/2020 6:54:20 AM.

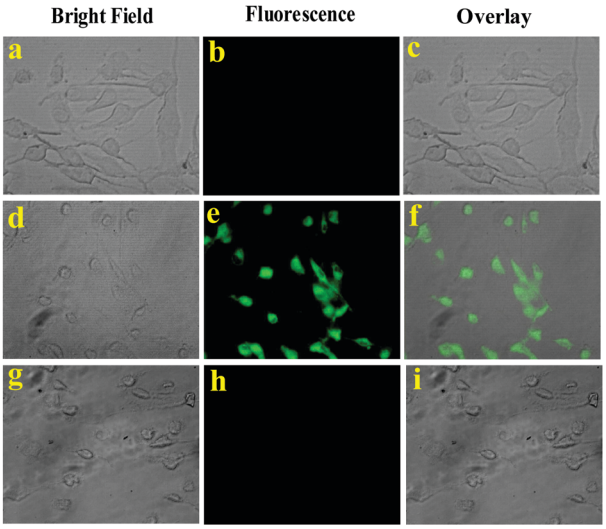

Fig. 9 Bright field, fluorescence and overlay images of Hep G2 cells. (a–c) The cells were incubated with 10 μM probe **L** for 30 min, (d–f) followed by addition and incubation with 10 μM Al^{3+} for another 30 min and (g–i) then with $NaHF_2$ for 30 min.

cells were treated with probe **L** (10 μM) for 30 min at 37 °C and then washed with PBS buffer to remove excess probe. After that, the treated cells were incubated with Al^{3+} ions (10 μM) for another 30 min at 37 °C. Then, these incubated cells were washed again with PBS buffer and images were recorded using a fluorescence microscope. Hep G2 cells treated with only probe **L** displayed no fluorescence signal, whereas an intense green fluorescence signal was detected in the intracellular area when stained with **L** followed by $Al(NO_3)_3$. Again, this bright fluorescence signal disappeared when the cells were treated with $NaHF_2$ (10 μM) solution (Fig. 9). Furthermore, there were no gross morphological changes in the bright-field images of the cells, suggesting that the cells remained viable throughout the imaging studies. The above results established the good cell-membrane permeability of **L** and that it could be employed in living cells for *in vitro* imaging of Al^{3+} and HF_2^- ions. Additionally, an MTT assay determined that probe **L** displayed very low cytotoxicity toward living cells (Fig. S14, ESI†).

Conclusions

In conclusion, we have successfully designed and synthesized a colorimetric and fluorometric probe, **L**, based on pyridine-dicarbohydrazide. Probe **L** shows both color and switch-on emission responses to Al^{3+} ions in organo aqueous solution as a result of the metal enhanced chelation effect (CHEF) inhibiting the PET, ESIPT and C=N isomerization processes. With a detection limit of 0.8 μM, this chemosensor displays high selectivity for Al^{3+} ions over 18 other commonly coexistent metal ions. The stoichiometry of **L**–Al^{3+} is determined to be 1 : 2 (**L** : Al^{3+}) and is confirmed by Job plot analysis. The association constant for **L** with Al^{3+} is found to be 4.26×10^4 M^{-2} on the basis of fluorescence studies, proposing a strong binding affinity for Al^{3+}. Besides, the *in situ* prepared **L**–2Al^{3+} complex can be utilized for the detection of HF_2^- ions *via* the displacement approach and it exhibits a "turn-off" type of fluorescence response. Moreover, the detection of Al^{3+} and HF_2^- ions was also carried out in Hep G2 cells to demonstrate the "off–on–off" fluorescence cellular image. It proves that the molecule penetrates into cells and thus it is applicable to biological systems. We anticipate that such cell imaging studies will be useful for Al^{3+} and HF_2^- ion related biological studies.

Experimental section

Materials and apparatus

All the chemical reagents and solvents (analytical and spectroscopic grades) were procured from commercial suppliers and used without additional purification. Millipore water was used throughout the experiment. Nitrate salts of Al^{3+} and Ag^+, chloride salts of metal ions (Na^+, K^+, Cr^{3+}, Cd^{2+}, Fe^{2+}, Zn^{2+}, Hg^{2+}, and Pb^{2+}) and perchlorate salts of metal ions (Ni^{2+}, Mn^{2+}, Cu^{2+}, Fe^{2+}, and Co^{2+}), terabutyl ammonium salts of F^-, Br^-, AcO^-, and HSO_4^- and sodium salts of HF_2^-, PPi, Pi, and NO_3^- were used for the experiments. Elemental analyses (C, H and N) were performed using a PerkinElmer 2400 Series-II CHNS, USA, elemental analyzer. ESI mass spectra were obtained using a Waters HRMS model XEVO-G2QTOF#YCA351 spectrometer. ^1H NMR and ^{13}C NMR spectra were obtained using a Bruker spectrometer (400 MHz) and ^1H NMR titration spectra were obtained using a Bruker spectrometer (300 MHz) with DMSO-d_6 solvent using trimethylsilane (TMS) as an internal standard. Fourier transform infrared (FT-IR) spectra were recorded on a PerkinElmer LX-1 FT-IR spectrophotometer (4000–400 cm^{-1}) by using a modern diamond attenuated total reflectance (ATR) accessory. UV-vis absorption spectra were obtained using a UV-1700 PharmaSpec UV-vis spectrophotometer (SHIMADZU). Fluorescence emission spectra were measured using a Horiba Jobin Yvon Fluoromax-4P spectrofluorometer. Single crystal structures (Fig. 1) were obtained using a single-crystal X-ray diffractometer (Bruker Smart Apex II). The cells were imaged by using a Zetasizer fluorescence microscope (Leica).

Calculations for the detection limit

The detection limit of **L** for Al^{3+} was calculated using the following equation:[28]

$$\text{Detection limit} = 3Sb1/S \quad (1)$$

where Sb1 is the standard deviation of the blank solution and S is the slope of the calibration curve.

Theoretical calculations

All the geometries for **L** and **L**–2Al^{3+} were optimized by density functional theory (DFT) calculations using the Gaussian 16 software package (basis set: B3LYP/6-31+G(d,p)). TDDFT calculations were also performed at the same level of theory.

Cell imaging studies

Cell line culture. Human liver cancer cell line Hep G2 cells and human lung fibroblast cells WI-38 were collected from the

Published on 10 July 2020. Downloaded by N-List College Programme on 9/9/2020 6:54:20 AM.

National Center for Cell Science (NCCS) Pune, India. The cells were grown in DMEM (Dulbecco's Modified Eagle Medium) with 10% FBS (Fetal Bovine Serum) and penicillin/streptomycin (100 units per ml) at 37 °C and 5% CO_2. All the treatments were performed at 37 °C and at a cell density allowing exponential growth.

Cell survivability assay. The cell survivability of the ligand was studied for human lung fibroblast cells WI38 following a reported procedure.[33] In brief, the viability of WI-38 cells after exposure to various concentrations of probe **L** was assessed by MTT assay. The cells were seeded in 96-well plates at 1×10^4 cells per well and exposed to probe **L** at concentrations of 0 μM, 20 μM, 40 μM, 60 μM, 80 μM, and 100 μM for 24 h. After incubation the cells were washed with 1 × PBS twice and incubated with MTT solution (450 μg ml^{-1}) for 3–4 h at 37 °C. The resulting formazan crystals were dissolved in an MTT solubilization buffer and the absorbance was measured at 570 nm by using a spectrophotometer (BioTek) and the value was compared with control cells.

Cellular imaging. According to a reported procedure, the Hep G2 cells were grown on a coverslip for more than 24 h. Then, the Hep G2 cells were treated with 10 μM of probe **L** for 30 min followed by addition and incubation with 10 μM $Al(NO_3)_3$ solution and then with $NaHF_2$ solution. The cells were washed with 1× PBS. Lastly, they were then mounted on a glass slide and fluorescence images were taken using a Leica fluorescence microscope.

Synthesis of bis(2-hydroxy-4-chlorobenzaldehyde)-2,6-pyridinedicarbohydrazone (L)

2,6-Pyridinedicarbohydrazide was synthesized following a reported method (Scheme 1).[25] A mixture of 2,6-pyridinedicarbohydrazide (0.19 g, 1.0 mmol) and 2-hydroxy-4-chlorobenzaldehyde (0.36 g, 2.3 mmol) was refluxed in methanol for 5 h. The light yellow solid formed was filtered off and dried in a vacuum (yield 0.39 g (84%), m.p. > 200 °C. Anal. calc. for $C_{21}H_{15}Cl_2N_5O_4$, C 53.41, H 3.20, N 14.83. Found: C 54.12, H 4.01, N 15.23%. ^{1}H NMR (400 MHz, DMSO-d_6): δ = 12.47 (s, 2H), 11.09 (s, 2H), 8.88 (s, 2H), 8.35 (d, J = 7.2 Hz, 2H), 8.28 (m, 1H), 7.92 (s, 3H), 7.75 (d, J = 2.4 Hz, 2H), 7.34 (m, 6.8 Hz, 2H), 6.97 (d, J = 8.8 Hz, 2H). ^{13}C NMR (100 MHz, DMSO-d_6): δ = 207.02 (for C═O of DMF), 162.79, 160.01, 156.46, 148.43, 147.17, 140.52, 131.64, 127.39, 126.22, 123.67, 121.48, 118.76, 31.17. IR (KBr, cm^{-1}): 3472, 3248, 1657, 1621, 1538, 1481, 1353, 1264, 1187, 1089, 1000, 950, 824, 716, 608, 560. ESI-MS: m/z 472.11, calcd for $[C_{21}H_{15}Cl_2N_5O_4 + H]^+$ 472.06. Crystals suitable for X-ray structural determination were obtained by slow evaporation of DMF solution.

Conflicts of interest

There are no conflicts to declare.

Acknowledgements

Samit Pramanik thanks Council of Scientific and Industrial Research (CSIR, File no. 09/096(0947)/2018-EMR-I), New Delhi, for a Junior Research Fellowship. The authors are thankful to Prof. Nitin Chattopadhyay and his scholar Mr Sinjan Das of Department of Chemistry, Jadavpur University, for the instrumental facility. SKM and SP thank Haldia Government College for the partial laboratory facility. DM is very much thankful to the DST, Government of India, for providing the INSPIRE Faculty Fellowship (DST/INSPIRE/04/2016/001948).

References

1 (*a*) S. Sen, T. Mukherjee, B. Chattopadhyay, A. Moirangthem, A. Basu, J. Marek and P. Chattopadhyay, *Analyst*, 2012, **137**, 3975–3981; (*b*) R. J. Lakowicz, *Principles of Fluorescence Spectroscopy*, Springer, New York, 3rd edn, 2006, p. xxvi; (*c*) A. P. de Silva, H. Q. N. Gunaratne, T. Gunnlaugsson, A. J. M. Huxley, C. P. McCoy, J. T. Rademacher and T. E. Rice, *Chem. Rev.*, 1997, **97**, 1515–1566; (*d*) B. Valeur and I. Leray, *Coord. Chem. Rev.*, 2000, **205**, 3–40.
2 R. A. Yokel, *Food Chem. Toxicol.*, 2008, **46**, 2261–2266.
3 S. H. Kim, H. S. Choi, J. Kim, S. J. Lee, D. T. Quang and J. S. Kim, *Org. Lett.*, 2010, **12**, 560–563.
4 D. Krewski, R. A. Yokel, E. Nieboer, D. Borchelt, J. Cohen, J. Harry, S. Kacew, J. Lindsay, A. M. Mahfouz and V. Rondeau, *J. Toxicol. Environ. Health, Part B*, 2007, **10**, 1–269.
5 M. J. Cullen, M. J. Allwood and D. M. Ambach, *Environ. Sci. Technol.*, 2012, **46**, 13048–13055.
6 (*a*) A. K. Mahapatra, S. S. Ali, K. Maiti, A. K. Manna, R. Maji, S. Mondal, M. R. Uddin, S. Mandal and P. A. Sahoo, *RSC Adv.*, 2015, **5**, 81203–81211; (*b*) T. Khan, S. Vaidya, D. S. Mhatre and A. Datta, *J. Phys. Chem. B*, 2016, **120**, 10319–10326.
7 (*a*) M. R. Wills and J. Savory, *Lancet*, 1983, **2**, 29–34; (*b*) C. A. Shaw and L. Tomljenovic, *Immunol. Res.*, 2013, **56**, 304–316; (*c*) G. Berthon, *Coord. Chem. Rev.*, 2002, **228**, 319–341.
8 (*a*) A. C. Alfrey, *Adv. Clin. Chem.*, 1983, **23**, 69–91; (*b*) A. M. Pierides, W. G. Edwards Jr, U. X. Cullum Jr, J. T. McCall and H. A. Ellis, *Kidney Int.*, 1980, **18**, 115–124; (*c*) T. P. Flaten, *Brain Res. Bull.*, 2001, **55**, 187–196; (*d*) M. Yasui, T. Kihira and K. Ota, *Neurotoxicology*, 1992, **13**, 593–600; (*e*) P. Nayak, *Environ. Res.*, 2002, **89**, 101–115.
9 (*a*) B. Wang, W. Xing, Y. Zhao and X. Deng, *Environ. Toxicol. Pharmacol.*, 2010, **29**, 308–313; (*b*) P. D. Darbre, *J. Inorg. Biochem.*, 2005, **99**, 1912–1919.
10 (*a*) C. S. Cronan, W. J. Walker and P. R. Bloom, *Nature*, 1986, **324**, 140–143; (*b*) J. Barcelo and C. Poschenrieder, *Environ. Exp. Bot.*, 2002, **48**, 75–92.
11 V. Kumar, A. Kumar, U. Diwan, R. Shweta and S. K. Srivastava, *Sens. Actuators, B*, 2015, **207**, 650–657.
12 M. Frankowski, A. Zioła-Frankowska and J. Siepak, *Talanta*, 2010, **80**, 2120–2126.
13 G. Tangen, T. Wickstrom, S. Lierhagen, R. Vogt and W. Lund, *Environ. Sci. Technol.*, 2002, **36**, 5421–5425.
14 M. Rezaee, Y. Yamini, A. Khanchi, M. Faraji and A. Saleh, *J. Hazard. Mater.*, 2010, **178**, 766–770.
15 A. Sanz-Medel, A. B. Soldado Caabezuelo, R. Milačič and T. Bantan Polak, *Coord. Chem. Rev.*, 2002, **228**, 373–383.

 This journal is © The Royal Society of Chemistry and the Centre National de la Recherche Scientifique 2020

Published on 10 July 2020. Downloaded by N-List College Programme on 9/9/2020 6:54:20 AM.

16 Y. C. Chen, I. L. Lee, Y. M. Sung and S. P. Wu, *Talanta*, 2013, **117**, 70–74.
17 (*a*) V. K. Gupta, A. K. Jain and P. Kumar, *Sens. Actuators, B*, 2006, **120**, 259–265; (*b*) V. K. Gupta, B. Sethi, N. Upadhyay, S. Kumar, R. Singh and L. P. Singh, *Int. J. Electrochem. Sci.*, 2011, **6**, 650–663; (*c*) V. K. Gupta, R. Jain and K. M. Pal, *Int. J. Electrochem. Sci.*, 2010, **5**, 1164–1178.
18 H. Wang, Z. Yu, Z. Wang, H. Hao, Y. Chen and P. Wan, *Electroanalysis*, 2011, **23**, 1095–1099.
19 (*a*) S. Samanta, B. Nath and J. B. Baruah, *Inorg. Chem. Commun.*, 2012, **22**, 98–100; (*b*) J. F. G. Reyes, P. O. Barrales and A. M. Diaz, *Talanta*, 2005, **65**, 1203–1208.
20 (*a*) J. C. Qin, L. Fan, T. R. Li and Z. Y. Yang, *Synth. Met.*, 2015, **199**, 179–186; (*b*) S. Sinha, B. Chowdhury and P. Ghosh, *Inorg. Chem.*, 2016, **55**, 9212–9220.
21 (*a*) A. Sahana, A. Banerjee, S. Lohar, B. Sarkar, S. K. Mukhopadhyay and D. Das, *Inorg. Chem.*, 2013, **52**, 3627–3633; (*b*) S. Kim, J. Y. Noh, K. Y. Kim, J. H. Kim, H. K. Kang, S.-W. Nam, S. H. Kim, S. Park, C. Kim and J. Kim, *Inorg. Chem.*, 2012, **51**, 3597–3602; (*c*) V. Saini, R. Krishnan and B. Khungar, *Photochem. Photobiol. Sci.*, 2020, **19**, 931–942; (*d*) P. Ghorai, K. Pal, P. Karmakar and A. Saha, *Dalton Trans.*, 2020, **49**, 4758–4773.
22 M. Wang, C. Cheng, C. Li, D. Wu, J. Song, J. Wang, X. Zhou, H. Xiang and J. Liu, *J. Mater. Chem. C*, 2019, **7**, 6767–6778.
23 (*a*) K. Ashley, A. Agrawal, J. Cronin, J. Tonazzi, T. M. McCleskey, A. K. Burrell and D. S. Ehler, *Anal. Chim. Acta*, 2007, **584**, 281–286; (*b*) T. L. Peters, T. J. Nestrlck, L. L. Lamparski and R. H. Sthel, *Anal. Chem.*, 1982, **51**, 2397–2398; (*c*) C. R. Wade, A. E. J. Broomsgrove, S. Aldridge and F. O. P. Gabbaï, *Chem. Rev.*, 2010, **110**, 3958–3984.
24 (*a*) K. Murugesan, V. Jeyasingh, S. Lakshminarayanan, S. Narayanan, S. Ramasamy, I. V. M. V. Enoch and L. Piramuthu, *Spectrochim. Acta, Part A*, 2019, **209**, 165–169; (*b*) A. Ghorai, S. S. Thakur and G. K. Patra, *RSC Adv.*, 2016, **6**, 108717–108725; (*c*) K. Dutta, R. C. Deka and D. K. Das, *J. Fluoresc.*, 2013, **23**, 823–828.
25 N. Yadav and A. K. Singh, *New J. Chem.*, 2018, **42**, 6023–6033.
26 (*a*) N. Xiao, L. Xie, X. Zhi and C. Fang, *Inorg. Chem. Commun.*, 2018, **89**, 13–17; (*b*) J. Wang and Y. Pang, *RSC Adv.*, 2014, **4**, 5845–5848; (*c*) S. K. Asthana, A. Kumar, Neeraj, Shweta, S. K. Hira, P. P. Manna and K. K. Upadhyay, *Inorg. Chem.*, 2017, **56**, 3315–3323.
27 (*a*) C. Yang, L. Liu, T. W. Mu and Q.-X. Guo, *Anal. Sci.*, 2000, **16**, 537–539; (*b*) H. A. Benesi and J. H. Hildebrand, *J. Am. Chem. Soc.*, 1949, **71**, 2703–2707; (*c*) Y. Shiraishi, S. Sumiya, Y. Kohono and T. Hirai, *J. Org. Chem.*, 2008, **73**, 8571–8574.
28 (*a*) L. L. Long, D. D. Zhang, X. F. Li, J. F. Zhang, C. Zhang and L. P. Zhou, *Anal. Chim. Acta*, 2013, **775**, 100–105; (*b*) T. Mandal, A. Hossain, A. Dhara, A. A. Masum, S. Konar, S. K. Manna, S. K. Seth, S. Pathak and S. Mukhopadhyay, *Photochem. Photobiol. Sci.*, 2018, **17**, 1068–1074.
29 R. Purkait and C. Sinha, *New J. Chem.*, 2019, **43**, 9815–9823.
30 (*a*) B. Miehlich, A. Savin, H. Stoll and H. Preuss, *Chem. Phys. Lett.*, 1989, **157**, 200–206; (*b*) A. D. Becke, *J. Chem. Phys.*, 1993, **98**, 5648–5662; (*c*) C. Lee, W. Yang and R. G. Parr, *Phys. Rev. B: Condens. Matter Mater. Phys.*, 1988, **B37**, 785–799.
31 M. J. Frisch, G. W. Trucks, H. B. Schlegel, G. E. Scuseria, M. A. Robb, J. R. Cheeseman, G. Scalmani, V. Barone, G. A. Petersson, H. Nakatsuji, X. Li, M. Caricato, A. V. Marenich, J. Bloino, B. G. Janesko, R. Gomperts, B. Mennucci, H. P. Hratchian, J. V. Ortiz, A. F. Izmaylov, J. L. Sonnenberg, Y. D. Williams, F. Ding, F. Lipparini, F. Egidi, J. Goings, B. Peng, A. Petrone, T. Henderson, D. Ranasinghe, V. G. Zakrzewski, J. Gao, N. Rega, G. Zheng, W. Liang, M. Hada, M. Ehara, K. Toyota, R. Fukuda, J. Hasegawa, M. Ishida, T. Nakajima, Y. Honda, O. Kitao, H. Nakai, T. Vreven, K. Throssell, J. A. Montgomery Jr, J. E. Peralta, F. Ogliaro, M. J. Bearpark, J. J. Heyd, E. N. Brothers, K. N. Kudin, V. N. Staroverov, T. A. Keith, R. Kobayashi, J. Normand, K. Raghavachari, A. P. Rendell, J. C. Burant, S. S. Iyengar, J. Tomasi, M. Cossi, J. M. Millam, M. Klene, C. Adamo, R. Cammi, J. W. Ochterski, R. L. Martin, K. Morokuma, O. Farkas, J. B. Foresman and D. J. Fox, *Gaussian 16, Revision C.01*, Gaussian, Inc., Wallingford CT, 2016.
32 (*a*) R. Purkait, A. Dey, S. Dey, P. P. Ray and C. Sinha, *New J. Chem.*, 2019, **43**, 14979–14990; (*b*) P. B. Thale, P. N. Borase and G. S. Shankarling, *Inorg. Chem. Front.*, 2016, **3**, 977–984.
33 (*a*) A. Samui, K. Pal, P. Karmakar and S. K. Sahu, *Mater. Sci. Eng., C*, 2019, **98**, 772–781; (*b*) K. Pal, S. Roy, P. K. Parida, A. Dutta, S. Bardhan, S. Das, K. Jana and P. Karmakar, *Mater. Sci. Eng., C*, 2019, **95**, 204–216.